Eur. Phys. J. D (2018) 72: 220
https://doi.org/10.1140/epjd/e2018-90234-4

THE EUROPEAN PHYSICAL JOURNAL D

Regular Article

Luminescence cross sections in the low-energy collisions of H^+, H_2^+, and H_3^+ ions with H_2

Ryszard Drozdowski[a] and Andrzej Kowalski

Institute of Experimental Physics, Faculty of Mathematics, Physics, and Informatics, University of Gdansk, ul. Wita Stwosza 57, 80-952 Gdansk, Poland

Received 17 May 2018 / Received in final form 12 August 2018
Published online 18 December 2018

Abstract. Luminescence cross sections for the optical emission of molecular hydrogen in the 200–600 nm spectral range and for the atomic Balmer-β line were measured for low-energy (≤1 keV) H^+, H_2^+, and H_3^+ ions colliding with H_2 gas targets. Molecular hydrogen transitions between singlet states were observed for all the systems studied, while the emission continuum H_2(a-b) and discrete spectra associated with other transitions between triplet states appeared only in the $H_2^+ + H_2$ collisions, where the spin conservation rule is fulfilled. Isotopic substitutions in the $H_2^+/D_2^+ + H_2$, D_2 system show that at $E_{lab} = 1$ keV, a dominant molecular luminescence mechanism is the collision-induced excitation (CIE) of the target.

1 Introduction

Electronic spectra of hydrogen molecule extend from vacuum ultraviolet (VUV), ultraviolet (UV), through the visible (VIS) spectral region, and into the infrared (IR) [1]. A detailed knowledge of many electronic transitions in H_2 reaches back almost a hundred years [2]. In the UV–VIS range, the most important spectral features of H_2 are a continuum due to the bound-free $H_2(a\,^3\Sigma_g^+ - b\,^3\Sigma_u^+)$ transition in the 120–600 nm region [3] and a discrete spectrum in the 350–800 nm region, consisting of many lines (on the order of tens of thousands [4]). The $H_2(a\,^3\Sigma_g^+ - b\,^3\Sigma_u^+)$ continuum was observed in laboratories, first in discharges and later in experiments using electron beams bombarding H_2 [5]. Emission of the continuum was observed also in the collisions of ground state Ar^+, Ne^+, Kr^+, Xe^+, and metastable Ar^{+*} ions with H_2 [6] and in the collisions of metastable $Ar^*(^3P_{0,1})$ atoms with H_2 [7]. The discrete parts of the H_2 VIS spectrum were mainly studied in discharges, and numerous electronic transitions were identified within the singlet and triplet systems [1,2,8]. A study of the multiline part of the H_2 spectrum under single-collision conditions is a challenge because these molecular lines appear very weak in comparison to atomic lines of the Balmer series and require long exposure times.

There is a great deal of interest in the application of H_2 emissions for the determination of conditions in various environments where collisions occur. Hydrogen continua appear in various spectral regions and their origins may differ; they can be due to recombination (Lyman, Balmer, and Paschen continuum), photoexcitation, or collision-induced excitation. The continua are of great interest in astrophysics (e.g., in the studies of solar flares [9], quasar emission [10], or in the observations of light from distant galaxies [11,12]). Spectroscopic analysis enables, for example, a determination of excitation mechanisms in galaxies [13] and a study of hydrogen molecular emission induced in a nebula by stellar winds [14]. Continuum emission serves also as a source of information in the spectral diagnostics of hydrogen-containing plasma [3,15,16]. There is currently some interest in collisional processes involving H_3^+ in the context of astrophysical models [17].

Important parameters in modeling low-pressure hydrogen plasma conditions are the excitation cross sections, σ^*, for H* and H_2* luminescence in the $H_n^+ + H_2$ collisions. The σ^* data for hydrogen atomic lines of the Balmer series are available for higher collision energies [18], while for energies below 1 keV some of the most trusted data are derived by extrapolation [19]. Luminescence cross sections for Balmer-β emitted in the $H_n^+ + H_2$ collisions at laboratory energies below 1 keV have been measured only once before [20] and were evaluated later to be incorrect by a factor of 30 [21]. Molecular hydrogen emission cross sections σ^* at low collision energies for the same systems were not known in 1992 [19] and we could not find anything in the literature published later; there are only measurements of σ^* for very small selected fragments of singlet spectra produced in $H^+ + H_2$ collisions above $E_{lab} = 150$ keV [22].

[a] e-mail: fizrd@ug.edu.pl

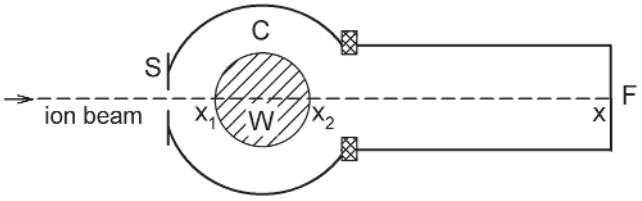

Fig. 1. A schematic construction of the collision cell (explanation in text).

2 Experimental

The vacuum part of the experimental apparatus consisted of three large (ca. 100 l) chambers pumped differentially (the arrangement is shown in Fig. 1 of Ref. [23]). In the first chamber, a hot-cathode Colutron ion source was installed on a 3D-adjustable mount. Hydrogen ions were generated from H_2 gas (Linde, purity 99.999%) or D_2 gas (Linde, purity 99%) at a relatively very high ion source pressure of 60 Pa, to minimize the amount of H_2^+ metastables [24]. The anode-to-cathode voltage U_A was kept mostly at 100 V, and occasionally set at 50 V to test a possible influence of residual metastable states of H_2^+ ions. Ions were extracted from the source by a 1000 V potential and transported to the second vacuum chamber, where they were mass-selected by a magnetic field separator. The first two vacuum chambers were independently pumped by two 1200 l/s oil diffusion pumps equipped with liquid nitrogen traps. Subsequently, the ions were transported to the third chamber, passing through electrostatic lenses and a retarder, where they were slowed down to a required energy before entering the collision cell. The collision chamber was pumped by two parallel 1400 l/s and 450 l/s turbomolecular pumps that provided a background pressure about 10^{-4} Pa during the measurements.

A schema of the collision cell as seen from above is shown in Figure 1. The cell (C) is cylindrical, with the beam slit (S) 1 mm wide and 8 mm high. The observation window (W), made of MgF_2, was mounted at the bottom, while a flexible tube supplying target gas was attached at the top of the cell. Hydrogen target gas was admitted into this 30 cm long, 2.5 cm i.d. tube, which simultaneously connected the scattering cell to an MKS Baratron capacitance manometer (head type 398 HD). The ion beam was collected in a Faraday cup (F) insulated from the collision cell (C). The available beam energies were in the 20–1000 eV range, with corresponding beam currents of 1–40 nA for H^+, 10–200 nA for H_2^+, and 5–180 nA for H_3^+, respectively. Ion currents were recorded continuously with a Keithley picoammeter and computer-averaged. The ion beam path in the collision cell was $x = 66$ mm, but only the region between $x_1 = 6$ mm and $x_2 = 18$ mm from the entrance slit was observed by the optical detection system. The bottom of the Faraday cup (F) was located relatively far away from the observation zone to avoid some background emission created by hydrogen ion beams bombarding a metal surface.

In most of our measurements, the target pressure was kept below 0.20 Pa, because in this range the luminescence intensity increased linearly with target gas pressure, while the ion beam current at 1 keV was attenuated by only 2–3% at $x = 66$ mm. Of the three ion projectiles, the total collision cross section at 1 keV is the largest for $H_2^+ + H_2$ (8×10^{-20} m^2 [19]). The mean free path at 0.20 Pa is then more than 20 cm and our experiment fulfills single collision conditions for all three systems studied. Higher target gas pressures (up to 2.0 Pa) were also applied for $H_2^+ + H_2$ collisions, to record molecular luminescence spectra with better resolution. Under these conditions, the intensity of light increased linearly with pressure, despite attenuation of the ion beam current up to 40% at $x = 66$ mm, a behavior that indicates some luminescence contribution from secondary collisions. We have recorded fragments of better-resolved (0.18 nm FWHM) molecular spectra for the $H_2^+ + H_2$ collisions at 1000 eV with both 0.19 and 2.0 Pa target gas pressures and found no important differences in the appearance of the spectra, apart from intensity variations (<50%) of some lines. To improve the signal-to-noise ratio and gain a 10-fold advantage in light collection time (the spectrum in the 350–600 nm range is compiled from 11 partially overlapping spectra of 46 nm span), we recorded the better resolved spectra at 2.0 Pa.

The luminescence from collision cell was reflected by an aluminum mirror toward the entrance slit of a spectrograph. The optical arrangement of our experiment is presented in Figure 1 of reference [25]. Luminescence spectra were recorded with a 1024-channel "Mepsicron" detector attached to a modified McPherson 218 spectrograph, which was equipped with 150, 300, 1200, and 2400 L/mm interchangeable snap-in gratings blazed at various wavelengths. The detector is sensitive only in the 200–600 nm spectral range. Its sensitivity profile was determined using a standard Osram Wi17/G tungsten ribbon lamp and a Hamamatsu L656K deuterium lamp [26]. The recorded luminescence signal at 0.19 Pa target gas pressure was from 1 to 30 cts/s, depending on the ion beam energy and the optical slit width used. The detector dark count rate was about 3 cts/s. The time necessary for collection of a luminescence spectrum varied from 20 min to 6 h. For $H_2^+ + H_2$, the luminescence spectra above 380 nm were always recorded with a cut-off filter absorbing light $\lambda < 380$ nm, to avoid a contribution of UV-light in the second order of a grating. At collision energies above 300 eV, some background light consisting mainly of the Balmer-β line was observed without target gas in the collision cell. The light disappeared completely when the ion beam was directed away from the collision cell; therefore, our conclusion is that this was caused by a beam neutralization on the edges of the entrance slit to the collision cell. The background light at collision energy of 1 keV did not exceed 20% of the luminescence recorded with target gas present and it was subtracted during cross section measurements.

A scaling of the measured luminescence intensity necessary to derive absolute cross sections was determined by performing measurements for the Balmer-β line in the $He^+ + H_2$ reaction at 700 eV [27]. In the course of our experiments, the volume of luminescence region observed in the collision cell and the solid angle of collection of light were the same as in the reference reaction. The calibration factor for σ^* was checked using another luminescent

reaction, namely, $H^+ + N_2$ at a beam energy of 1000 eV [28] and we found a very small discrepancy between the results of both normalizations.

Experimental uncertainties of σ^* in the excitation functions presented below are standard deviations from averages of 10–15 measurements at each collision energy. Systematic errors are certainly present. First of all, they may stem from uncertainty of the value of σ^* determined in reference [27], which we take as a reference (there is only a limited discussion of this problem in Ref. [27], where uncertainties in relative cross sections are estimated to be 10% or less). The absolute values for Balmer-β may contain systematic errors due to the manufacturers' scaling of electronic instruments measuring ion intensity and target gas pressure. The values of σ^* for the H_2* emission may have additional systematic error resulting from uncertainty of the detector sensitivity curve which served for correction of the recorded spectra. We estimate that this latter error should not exceed 20%.

3 Luminescence spectra

Luminescence spectra resulting from collisions of $H_n{}^+$ with H_2 at 1 keV beam energy are shown in Figure 2.

The spectra are corrected for wavelength-dependent sensitivity of the detection system. Atomic lines H_β and H_γ of the Balmer series stand out in all three spectra. In the neighborhood of the Balmer series, numerous densely packed rovibronic lines of H_2 appear. The wavelengths of (v',v'') bands belonging to the strongest electronic singlet transition H_2(GK $3d\sigma\ {}^1\Sigma_g{}^+ -$ B $2p\sigma\ {}^1\Sigma_u^+$) are marked in Figure 1a (GK has been earlier denoted as G [1,2]). The lowest bound triplet state of molecular hydrogen is H_2(c $2p\pi\ {}^3\Pi_u$), which is metastable ($\tau = 95$ μs [29]). Slightly higher, by just 0.023 eV [29], lies the H_2(a $2s\ {}^3\Sigma_g{}^+$) state, which has a much shorter radiative lifetime, reported as $\tau = (10.45 \pm 0.25)$ ns from experiment [30] and as $\tau = 8.8$ ns from theory [29]. This state decays to the repulsive H_2(b $2p\sigma\ {}^3\Sigma_u{}^+$) state and the spectrum associated with this transition is the most intense one, extending from λ120 nm to about λ600 nm [3]. A large part of the continuum can be seen in Figure 2b (note that the detection efficiency falls to zero below λ190 nm, with the onset of absorption of light in air). So-called 0-0 bands, i.e., the wavelengths of $(v' = 0 \rightarrow v'' = 0)$ for numerous other triplet transitions from higher states down to the a and c states [1] are marked in Figure 2b (the energy of the upper electronic state increases toward shorter wavelengths). Among the triplet transitions in Figure 2b, one can recognize relatively intense bands in the λ560–610 nm region. The emissions below λ460 nm, expected to be much weaker than those from lower triplet states, are obscured by singlet transitions and could not be identified. The spin-conservation rule permits formation of H_2* triplet states only for the $H_2{}^+ + H_2$ system and the validity of this rule is confirmed in Figure 2, where the triplet transitions are absent for the H^+ and $H_3{}^+$ ion projectiles.

A spectrum recorded for $H_2{}^+ + H_2$ with better spectral resolution is presented in Figures 3–5. One can identify rovibronic lines of transitions between electronic singlet states: H_2(GK $3d\sigma\ {}^1\Sigma_g{}^+ -$ B $2p\sigma\ {}^1\Sigma_u^+$), H_2(I $3d\pi\ {}^1\Pi_g -$ B $2p\sigma\ {}^1\Sigma_u^+$), and H_2(H$\overline{\text{H}}$ $3s\sigma\ {}^1\Sigma_g{}^+ -$ B $2p\sigma\ {}^1\Sigma_u^+$). The H_2(GK-B) transition appears clearly for all three ion projectiles $H_n{}^+$, the other two transitions could not be identified for $H^+ + H_2$ and $H_3{}^+ + H_2$ due to lower intensity of molecular luminescence. The wavelengths of (v',v'') bands in H_2(GK-B) [2] are marked in Figures 3–5. References [2,31] describe the R2 (λ463.403 nm) rotational line of H_2(GK-B) ($v' = 0$, $v'' = 0$) as the strongest in the molecular spectrum of hydrogen in the VIS. The observed triplet transitions in the λ560–610 nm range (Fig. 5) are due to emissions from the H_2(g $3d\sigma\ {}^3\Sigma_g^+$, h $3s\sigma\ {}^3\Sigma_g^+$, i $3d\pi\ {}^3\Pi_g$, j $3d\delta\ {}^3\triangle_g$) states to the H_2(c $2p\pi\ {}^3\Pi_u$) state and contain a small part of the Fulcher band H_2(d $3p\pi\ {}^3\Pi_u -$ a $2s\ {}^3\Sigma_g{}^+$), which extends above λ600 nm.

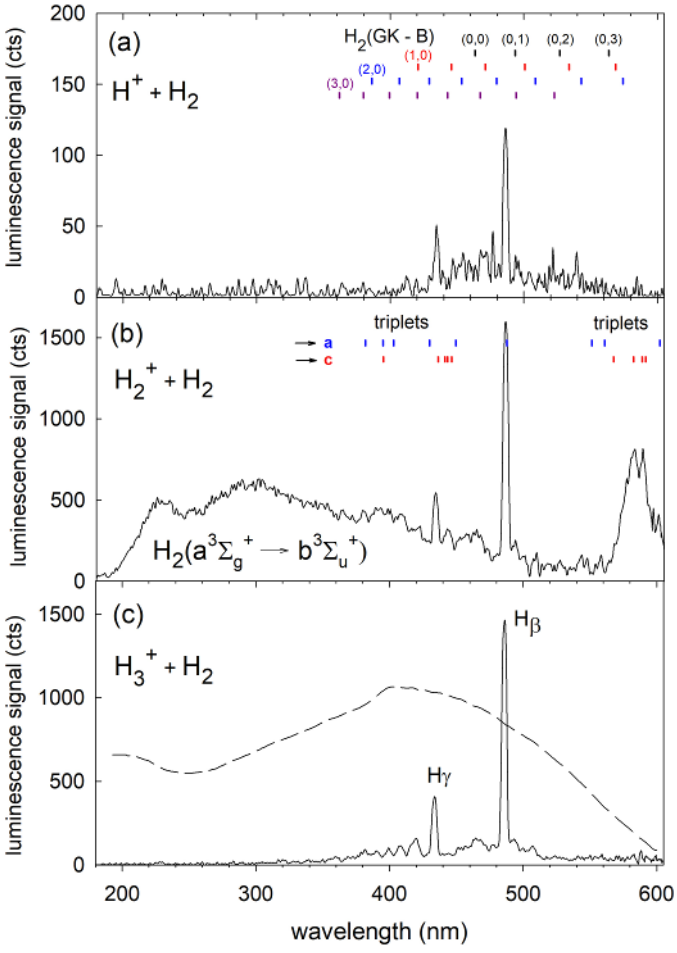

Fig. 2. Overview spectra taken at ion beam energy of 1 keV, target gas pressure 0.19 Pa, spectral resolution 4 nm FWHM. The spectra are corrected for wavelength-dependent sensitivity of the detection system, shown as a dashed line in part (c). In part (a), known vibrational transitions (v',v'') of the strongest spectrum H_2(GK-B) [2] are marked; in part (b), known $(v' = 0 \rightarrow v'' = 0)$ transitions from various higher triplet states to the two lowest (a and c) triplet states of H_2 are indicated [1].

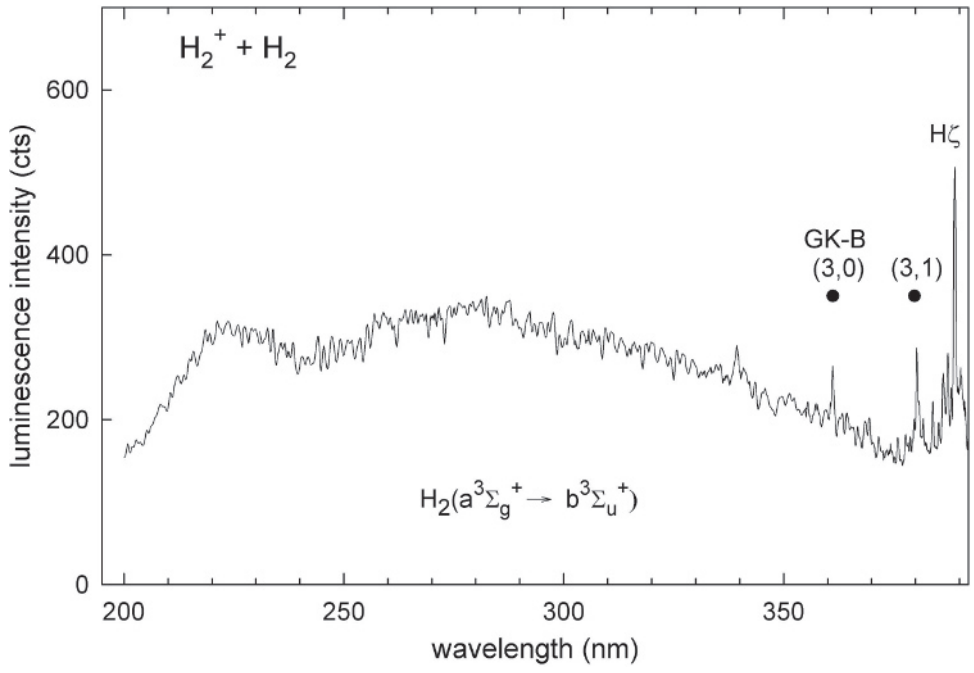

Fig. 3. Luminescence spectrum recorded at 1 keV beam energy for $H_2^+ + H_2$ in the λ190–392 nm region; resolution 0.5 nm (up to λ375 nm) and 0.18 nm FWHM (above λ375 nm); target gas pressure 2.0 Pa. The spectrum is corrected for sensitivity of the optical detector.

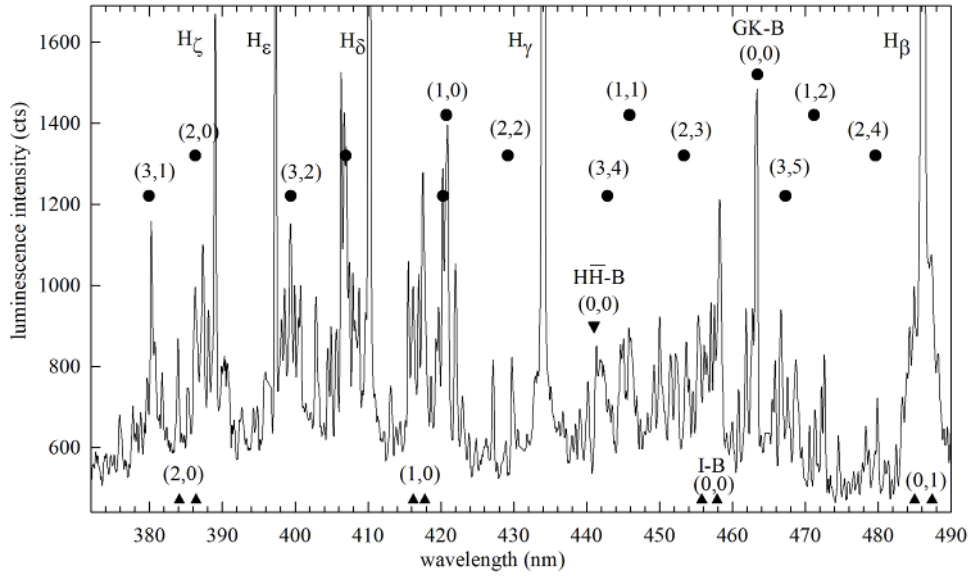

Fig. 4. Luminescence spectrum recorded at 1 keV beam energy for $H_2^+ + H_2$ in the λ372–490 nm region (resolution 0.18 nm, target gas pressure 2.0 Pa). The peak of H_β reaches 31500 cts. The spectrum is corrected for sensitivity of the optical detector. Positions of the strongest rovibronic lines of the GK-B, I-B, and HH̄-B electronic transitions in H_2 molecule are shown as full circles, triangles pointing up, and triangles pointing down, respectively.

The mechanism of excitation of the Balmer-β line likely varies with collisional system. For $H^+ + H_2$ (see the energy diagram in Fig. 6, left column), among exit channel leading to H_β*, the lowest one involves electron transfer to the projectile, while collisional dissociation of the target with simultaneous excitation of H_β* is more endoergic. For $H_2^+ + H_2$ (the middle column in Fig. 6), the lowest H_β* product channel corresponds to proton transfer from the projectile ion to the target. More endoergic channels, namely, collisional dissociation of the projectile and collisional dissociation of the target can also produce H_β*. To check which pathway is more effective at 1 keV ion beam energy, we have measured the D_β/H_β intensity ratio for $H_2^+ + D_2$ and $D_2^+ + H_2$ systems using isotopic spectral shift. The ratio is equal to (0.36 ± 0.03) and (1.13 ± 0.05), respectively.

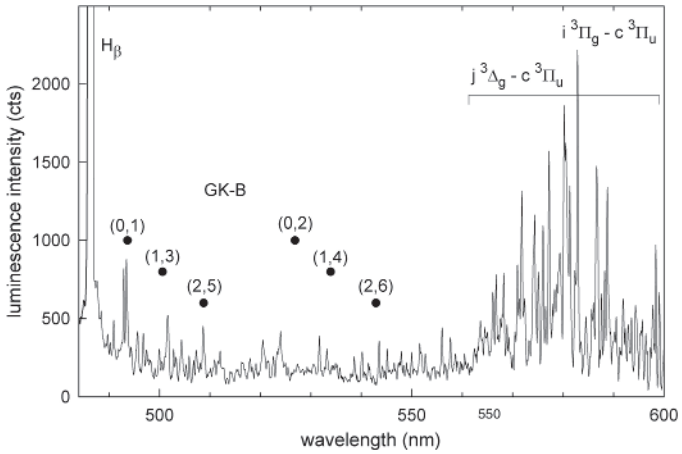

Fig. 5. Luminescence spectrum observed at 1 keV beam energy for $H_2^+ + H_2$ in the λ484–600 nm region (resolution 0.18 nm, target gas pressure 2.0 Pa). The spectrum is corrected for sensitivity of the optical detector. Positions of the strongest vibrational lines of H_2(GK-B) transition are shown as full circles.

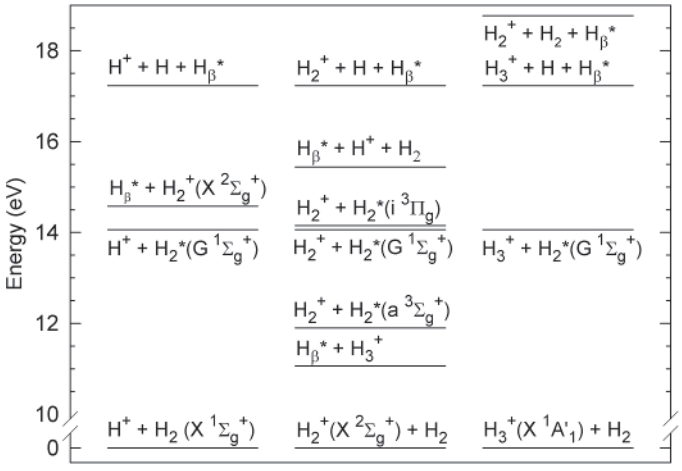

Fig. 6. Energy diagram for the lowest levels of the $H_n^+ + H_2$ systems, based on data from references [1,32].

This seems to indicate that the excited hydrogen atom arises more often from the projectile than from the target, reflecting energy ordering of the product channels. A similar trend for this reaction was observed in [21] for H_α radiation, where the projectile and target atoms were distinguished by Doppler shift of atomic lines. For the $H_3^+ + H_2$ system, the lowest energy levels are given in the right column in Figure 5. Exit channels associated with excitation of Balmer-β lines are more endoergic than in the case of two other projectile ions. The lowest channel here is associated with collisional dissociation of the target; a slightly higher channel corresponds to rather complicated (and therefore less probable) ejection of an excited atom by H_3^+ projectile ion. Measurements of D_β/H_β intensity ratio for $H_3^+ + D_2$ and $D_3^+ + H_2$ systems gave (0.91 ± 0.05) and (0.82 ± 0.05), respectively. The similarity of these results indicates that very likely the excitation of the Balmer-β line occurs here via some even higher channels, corresponding to more complete collisional dissociation into atoms.

4 Luminescence cross sections: Balmer-β line

The luminescence cross sections were obtained from the sums of photons attributed to the Balmer-β line. Only the spectra obtained for low (0.19 Pa) target gas pressure were used in cross section measurements. To collect these spectra, we used a low spectral resolution (4.0 nm FWHM).

4.1 $H^+ + H_2$

The excitation function for production of H_β is presented in Figure 7. The $\sigma^*(H_\beta)$ value increases monotonically from 0.0035×10^{-22} m^2 at 200 eV to 0.028×10^{-22} m^2 at 1000 eV. It can be compared with $\sigma^*(H_\beta) = 0.07 \times 10^{-22}$ m^2 at 1200 eV, which can be derived from Figure 1 of reference [33]. Reference [20] at 1 keV gives $\sigma^*(H_\beta) = 0.009 \times 10^{-22}$ m^2, three times lower than our result. The discrepancy may be due to important differences in experimental arrangements and procedures. In reference [20], ion current was four orders of magnitude higher than in the present work, light was collected on the ion beam axis using an original calibration of emission intensity, and target gas pressure was measured with an ionization gauge. The results of [20] were evaluated later [21] to be too low by a factor of 30, which is true at 3 keV, but seems exaggerated for collision energies below 1 keV. For the Balmer series, the review of Phelps [19] gives only the values of $\sigma^*(H_\alpha)$ from reference [21] and extrapolates them below 1.5 keV down to 100 eV. Assuming that the ratio of intensities H_α/H_β in this collision energy range is about 5 [20], one obtains $\sigma^*(H_\beta) = 0.5 \times 10^{-22}$ m^2 at 1 keV. Our result is then about 20 times lower than the extrapolation made by Phelps.

4.2 $H_2^+ + H_2$

In the present work, $\sigma^*(H_\beta) = 0.125 \times 10^{-22}$ m^2 at 1 keV and σ^* decreases toward lower collision energies (see Fig. 7). To compare this with earlier results, we took the extrapolations of reference [19] for H_α cross sections measured above 2 keV [21] and assumed an H_α/H_β intensity ratio of 5. In this way, one obtains $\sigma^*(H_\beta) = 0.5 \times 10^{-22}$ m^2 at 1000 eV, four times higher than our result. Reference [20] gives measured $\sigma^*(H_\beta) = 0.04 \times 10^{-22}$ m^2 at 1 keV, three times lower than our result. The latter discrepancy probably has the same causes as given in Section 4.1, namely, different experimental arrangements and procedures.

4.3 $H_3^+ + H_2$

The excitation function is presented in Figure 7. At 1 keV we have measured $\sigma^*(H_\beta) = 0.146 \times 10^{-22}$ m^2. Phelps [19] used the experimental data above 3 keV for H_α [21] and extrapolated the excitation function toward lower

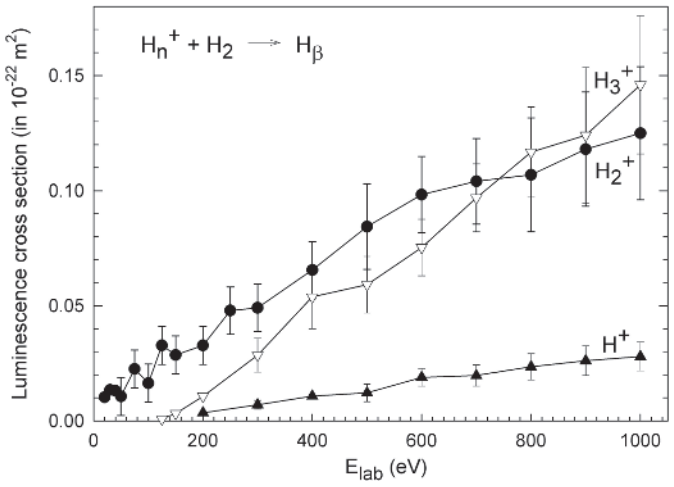

Fig. 7. Excitation functions for H_β luminescence resulting from collisions of H_n^+ with H_2 at target gas pressure of 0.19 Pa. Symbols used are as follows: for H^+ – full triangles, for H_2^+ – full circles, for H_3^+ – triangles.

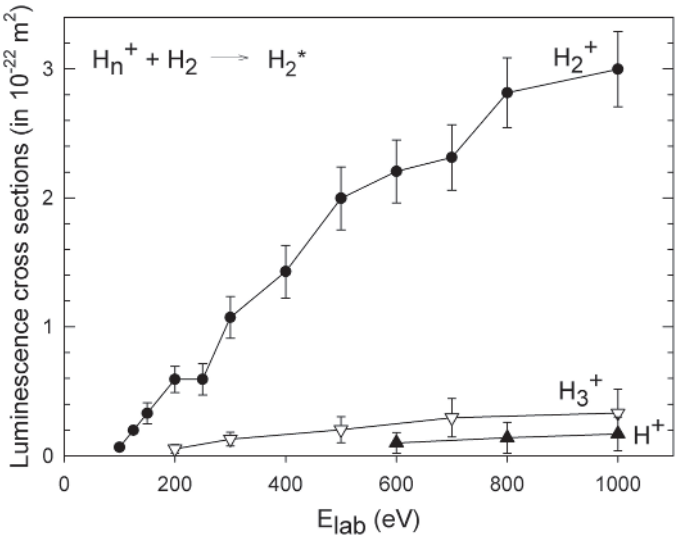

Fig. 8. Excitation functions for H_2^* luminescence in the λ190–600 nm spectral region, determined for collisions of H^+ (full triangles), H_2^+ (full circles), and H_3^+ (triangles) with H_2. Target gas pressure was equal to 0.19 Pa in all measurements.

energies. Assuming an H_α/H_β intensity ratio equal to 5, one obtains an estimate $\sigma^*(H_\beta) = 1.3 \times 10^{-22}$ m^2 at 1000 eV [19]. Our experimental result is about an order of magnitude lower than this estimate by extrapolation.

The excitation functions for $H_2^+ + H_2$ and $H_3^+ + H_2$ are somewhat different, probably reflecting the differences in mechanisms of production of atomic luminescence in both cases. The formation of H_β in $H_2^+ + H_2$ collisions occurs in the lowest exit channel $H_\beta + H_3^+$, endoergic by 11 eV and corresponding to the proton transfer that leaves the H atom of the projectile excited (see Fig. 6, middle column). As the excitation function shows, the Balmer series in this case can be observed from the lowest collision energy $E_{lab} = 20$ eV, which in the center-of-mass frame corresponds to $E_{CM} = 10$ eV. This small (1 eV) deficiency of energy can be supplied from the collision energy spread caused by thermal motion of the target gas (Chantry effect [34]).

Tables 4 and 6 of reference [19] contain measured $\sigma^*(H_\alpha)$ for $H_2^+ + H_2$ and $H_3^+ + H_2$ in the 2–10 keV collision energy range [21]. The luminescence cross sections for H_3^+ projectiles at these energies are always about 20% higher than for H_2^+. Below 2 keV, the values of $\sigma^*(H_\alpha)$ for both collision systems were extrapolated and at 750 eV, the numbers differ by a factor of 4.6 in favor of the H_3^+ precursor [19]. The relative intensity $(H_\alpha)/(H_\beta)$ is approximately constant around $E_{coll} \sim 1$ keV (as measured in numerous experiments); therefore, the trends in excitation functions for H_α and H_β should be very similar. Our results for H_β disagree with the extrapolations made in reference [19]. From Figure 7, one can see that at $E_{coll} = 750$ eV both projectiles have the same $\sigma^*(H_\beta)$ (contrary to the claim made in Ref. [19]) and from this energy on, the slightly higher yield of H_3^+ projectiles confirms the trend observed in reference [21] at higher collision energies. It seems a plausible explanation that the intensity of the Balmer-β line for $H_3^+ + H_2$ is slightly higher than for $H_2^+ + H_2$ above 1 keV, because in this energy range a complete dissociation into excited atoms plays a bigger role. This mechanism favors a system with more hydrogen atoms (in this case $i = 5$ vs. $i = 4$, which is close to the observed factor 1.2).

5 Molecular luminescence cross sections $\sigma(H_2^*)$

5.1 $H^+ + H_2$

In our studies at low target gas pressure (0.19 Pa), the H_2^* emission can be clearly recognized only in the spectral region around H_β and H_γ, where the strongest bands of H_2(GK-B) are located. Beyond the λ400–560 nm region, molecular luminescence was indistinguishable from the background recorded without target gas. In the literature we could not find absolute cross sections for excitation of UV–VIS luminescence of a hydrogen molecule induced by H^+ impact at 1 keV. There are only approximate cross sections at collision energies ≥150 keV [22], concerning two fragments of discrete molecular spectra of H_2, namely, the H_2(G-B) (0,0) and H_2(I-B) (0,0) bands measured with 1.6 nm bandpass filter at λ463.2 nm and λ417.6 nm, respectively. The cross sections at 150 keV are about 1×10^{-24} m^2 for each band and the excitation functions rapidly decrease when the collision energy becomes higher. Our measurements give $\sigma(H_2^*) = 0.17 \times 10^{-22}$ m^2 at 1 keV. The excitation function is presented in Figure 8; it rises slowly with ion beam energy. Molecular hydrogen luminescence for $H^+ + H_2$ was earlier observed in VUV [35], and the cross section for emission of Lyman bands around λ160 nm, on the rising part of the excitation function, measured at 20 keV was found to be $\sigma(H_2^*) = 3.4 \times 10^{-22}$ m^2 [35].

Table 1. Luminescence cross sections for hydrogen molecular emission in the 200–600 nm range and for the Balmer-β atomic line measured relative to the value for the $H_2^+ + H_2$ system (uncertainty 10%). Target gas pressure = 0.19 Pa.

Projectile ion + target	Collision energy E_{lab} (eV)	Collision energy E_{CM} (eV)	Molecular hydrogen emission $\sigma(H_2^*,D_2^*)$	Atomic emission σ^*(Balmer-β)	$\sigma^*(D_\beta)/\sigma^*(H_\beta)$
$H_2^+ + H_2$	1000	500	1.00	1.00	
$H_2^+ + D_2$	1000	667	1.02	0.96	0.36
$D_2^+ + D_2$	1000	500	0.46	0.41	
$D_2^+ + H_2$	1000	333	0.64	0.75	1.13

5.2 $H_2^+ + H_2$

Our result for luminescence cross section is $\sigma(H_2^*) = 3.0 \times 10^{-22}$ m^2 at 1 keV (see Fig. 8) and of this value we attribute 75% to the triplet H_2(a-b) continuum, 13% to all transitions between singlet states producing discrete emission in the λ380–560 nm region, and 12% to the triplet discrete spectra in the λ560–610 nm spectral range. This cross section can be compared only with $\sigma(H_2^*) = 10 \times 10^{-22}$ m^2 measured for excitation of the triplet continuum H_2(a-b) when 15 eV electrons bombarded H_2 [36].

Experimental cross sections are available for the H_2^* (a-b) continuum emission between λ170 nm and λ360 nm for $Ar^+ + H_2$ colliding at $E_{CM} = 19$ eV and for metastable $Ar^{+*} + H_2$ at $E_{CM} = 0.5$ eV. The values are believed to be accurate within a factor of 3 and they are equal to 0.04×10^{-22} m^2 and 1.4×10^{-20} m^2, respectively [6]. For both argon ions colliding with H_2, production of triplet states is allowed by the spin-conservation rule. The enormous H_2^*(a-b) luminescence cross section for $Ar^{+*} + H_2$ is explained by an accidental resonance of the metastable states of Ar^{+*} with molecular excited levels of H_2 [6].

We have measured relative luminescence cross sections for various isotopic combinations of the diatomic projectile ion–target systems. The results are collected in Table 1. Additional spectra recorded with higher resolution at 1 keV show that molecular lines associated with the isotope used as a target greatly outnumber those arising from the projectile. This indicates that at this collision energy, collision-induced excitation (CIE) of the target dominates over charge transfer.

5.3 $H_3^+ + H_2$

The cross section for molecular hydrogen emission observed for this system is $\sigma(H_2^*) = 0.33 \times 10^{-22}$ m^2 at 1000 eV. There is no recognizable molecular emission below 200 eV collision energy, and at higher energies, the excitation function slowly rises with E_{coll} up to 1 keV (see Fig. 8).

6 Conclusions

Luminescence spectra observed in the collisions of H_n^+ ions with H_2 at energies up to 1 keV show important differences caused by the spin properties of the projectiles. The $H_2^+ + H_2$ system fulfills the spin conservation rule permitting formation of electronically excited H_2^* triplet states and this leads to a considerably larger molecular luminescence cross section. The measured cross section for molecular H_2^* emission for $H_2^+ + H_2$ at 1 keV is $\sigma(H_2^*) = 3 \times 10^{-22}$ m^2, an order of magnitude higher than for the other two projectiles. Triplet emissions of H_2^* excited in $H_2^+ + H_2$ collisions dominate the spectrum in the λ200–600 nm region, contributing about 87% of the light. The remaining 13% of emission is from singlet H_2^* states. This fraction of the value of the entire $\sigma(H_2^*)$ from $H_2^+ + H_2$ is approximately equal to $\sigma(H_2^*)$ of luminescence produced in the $H_3^+ + H_2$ system, where the excitation of triplet transitions is forbidden. This indicates that both molecular projectiles excite singlet molecular states of hydrogen with similar yield.

The Balmer-β emission cross sections at 1 keV are on the order of 10^{-23} m^2 for H_2^+ and H_3^+ projectiles, while for H^+ they are about five times lower. Below $E_{coll} = 750$ eV, the $\sigma^*(H_\beta)$ cross section for H_2^+ projectile is slightly larger than for H_3^+, at higher collision energies the ordering reverses. Isotopic substitutions show that for $H_2^+ + H_2$, a dominant mechanism of luminescence at 1 keV is CIE of the target.

The velocities of H_n^+ ions at 1 keV are between 250 and 440 km/s, overlapping with typical velocities of solar winds, which are in the 200–400 km/s range [37]. Therefore, luminescence cross sections obtained in the present work can be useful for making estimates of light intensity produced in collisions of solar wind with hydrogen molecules. The presence and relative strength of the UV emission continuum or VIS triplet emissions can be used as a simple indicator of H_2^+ participation in the populations of stellar winds.

This work was financed within the statutory funds of the University of Gdańsk: DS-530-5200-D464-16, DS-530-5200-D464-17, and DS-530-5200-D464-18.

Author contribution statement

Both authors contributed equally to the paper.

References

1. K.P. Huber, G. Herzberg, *Molecular Spectra and Molecular Structure. IV. Constants of Diatomic Molecules* (Van Nostrand, New York, 1979)
2. O.W. Richardson, *Molecular Hydrogen and Its Spectrum* (Yale University Press, London, 1934)
3. U. Fantz, B. Schalk, K. Behringer, New J. Phys. **2**, 7 (2000)
4. G.H. Dieke, J. Mol. Spectrosc. **2**, 494 (1958)
5. A.S. Coolidge, Phys. Rev. **65**, 236 (1944)
6. D. Brandt, C. Ottinger, Phys. Rev. A **19**, 219 (1979)
7. C.R. Lishawa, J.W. Feldstein, T.N. Stewart, E.E. Muschlitz, J. Chem. Phys. **83**, 133 (1985)
8. H.M. Crosswhite, ed., *The Hydrogen Molecule Wavelength Tables of Gerhard Heinrich Dieke* (Wiley-Interscience, New York, 1972)
9. P. Heinzel, L. Kleint, Astrophys. J. Lett. **794**, L23 (2014)
10. J. Kwan, J.H. Krolik, Astrophys. J. **233**, L91 (1979)
11. D. Maoz et al., Astrophys. J. **404**, 576 (1993)
12. B.M. Peterson, et al., Astrophys. J. **368**, 119 (1991)
13. H. Mouri, Astrophys. J. **427**, 777 (1994)
14. A.N. Witt, T.P. Stecher, T.A. Boroson, R.C. Bohlin, Astrophys. J. **336**, L21 (1989)
15. B.P. Lavrov, A.S. Melnokov, M. Känning, J. Röpcke, Phys. Rev. E **59**, 3526 (1999)
16. A. Pospieszczyk, Phys. Scr. **T119**, 71 (2005)
17. T. Oka, Philos. Trans. R. Soc. A **370**, 4991 (2012)
18. E.W. Thomas, *Excitation in Heavy Particle Collisions* (Wiley-Interscience, New York, 1972)
19. A.V. Phelps, J. Phys. Chem. Ref. Data **19**, 653 (1990)
20. W.R. Hess, Phys. Rev. A **9**, 2036 (1974)
21. I.D. Williams, J. Geddes, H.B. Gilbody, J. Phys. B **15**, 1377 (1982)
22. J.L. Edwards, E.W. Thomas, Phys. Rev. **165**, 16 (1968)
23. A. Ławicki, B. Pranszke, A. Kowalski, Ch. Ottinger, Nucl. Instrum. Methods Phys. Res. B **259**, 861 (2007)
24. J.J. Leventhal, L. Friedman, J. Chem. Phys. **50**, 2928 (1969)
25. A. Ehbrecht, A. Kowalski, Ch. Ottinger, Int. J. Mass Spectrom. Ion Process. **156**, 41 (1996)
26. T. Glenewinkel-Meyer, B. Müller, C. Ottinger, H. Tischer, J. Chem. Phys. **88**, 3475 (1988)
27. R.C. Isler, R.D. Nathan, Phys. Rev. A **6**, 1036 (1972)
28. B. Van Zyl, M.W. Gealy, H. Neumann, Phys. Rev. A **28**, 2141 (1983)
29. U. Fantz, D. Wünderlich, Atom Data Nucl. Data **92**, 853 (2006)
30. G.C. King, F.H. Read, R.E. Imhof, J. Phys. B **8**, 665 (1975)
31. W. Kapuścinski, J.G. Eymers, Proc. R. Soc. Lond. A **119**, 83 (1928)
32. A.A. Radzig, B.M. Smirnov, *Reference Data on Atoms, Molecules and Ions* (Springer, Berlin, 1985)
33. D.H. Loyd, H.R. Dawson, Phys. Rev. A **11**, 140 (1975)
34. P.J. Chantry, J. Chem. Phys. **55**, 2746 (1971)
35. D.A. Dahlberg, D.K. Anderson, I.E. Dayton, Phys. Rev. **170**, 127 (1968)
36. N. Böse, J. Phys. B **11**, L83 (1978)
37. S.L. McGregor et al., J. Geophys. Res. **116**, A03101 (2011)